The Chemical Vapor Deposition of Aluminum Nitride: Unusual Cluster Formation in the Gas Phase

Alexey Y. Timoshkin, Holger F. Bettinger, and Henry F. Schaefer, III*

Contribution from the Department of Chemistry, Inorganic Chemistry Group, St. Petersburg State University, University Prospect 2, 198904, Old Peterhof, St. Petersburg, Russia, and Center for Computational Quantum Chemistry, University of Georgia, Athens, Georgia 30602

Received December 3, 1996. Revised Manuscript Received March 14, 1997[⊗]

Abstract: An *ab initio* investigation of the chemical vapor deposition of AlN from the $AlCl_3NH_3$ adduct is presented. Geometries, harmonic vibrational frequencies and relative energies for the $AlCl_3NH_3$ adduct, its dissociation products $AlCl_n$, NH_n ($n = 1-3$), and ring and cluster compounds [$(Cl_2AlNH_2)_n$ ($n = 1, 2$), $(ClAlNH)_n$ ($n = 1, 2, 3, 4, 6$)] are discussed. The Al−N bond lengths in the investigated compounds are strongly dependent on the coordination numbers of the aluminum and nitrogen centers, decreasing from 2.0 Å for 4-coordinated Al/N centers to 1.79 and 1.68 Å for 3- and 2-coordinated Al/N centers, respectively. Thermodynamic analysis shows that dissociation of Cl_xAlNH_x ($x = 2, 3$) compounds with elimination of HCl and simultaneous formation of oligomeric forms is preferable to the process of dissociation into components or simple HCl detachment. Under standard conditions gaseous 4-coordinated Al/N compounds $(ClAlNH)_6$ and $(ClAlNH)_4$ are more stable than 3-coordinated $(ClAlNH)_2$ and $(ClAlNH)_3$ compounds. In 4-membered rings and clusters, the electrostatic repulsion between nearby Al−Al and N−N atoms makes reorganization to 6-membered rings extremely favorable. The suggested mechanism of AlN deposition involving cluster formation in the gas phase is discussed.

Introduction

The chemical vapor deposition (CVD) technique is widely used to produce prospective materials such as aluminum nitride for the microelectronics industry. High thermal conductivity, large energy gap, good thermal stability, and chemical inertness of aluminum nitride make it an advanced ceramic material and a suitable dielectric for semiconductor devices.[1−3] Organoaluminium compounds have been used as precursors for aluminum nitride;[4−7] however, the product formed has a high degree of carbon contamination due to pyrolysis of the organic substituents and is not suitable for commercial use. The CVD of aluminum chloride and ammonia is well studied and yields high purity AlN.[1−3,8−12] Despite the fact that this process has been the subject of numerous experimental studies, the chemical nature of the intermediates in AlN growth is still unknown. It has been shown that, together with formation of AlN films, some particles are formed in the gas phase.[8] Formation of clusters, ranging in size from 0.8 nm (700 °C) to 0.5 nm (1100 °C) was found to be a key process in the rapid growth of AlN.[9] However, the "large number of chemical species existing in the gas phase as a result of chemical reactions makes it difficult to say what is actually a significant growth species among them."[9]

In order to characterize the growth species involved in the CVD of AlN *via* gas phase reactions between aluminum chloride and ammonia, we have carried out *ab initio* investigations of possible precursors for cluster formation.

The chemical vapor deposition process starts with formation of the $AlCl_3NH_3$ adduct.[9] As the temperature increases, two thermal dissociation processes can take place: dissociation of the adduct

$$AlCl_3NH_3(g) \rightleftarrows AlCl_3(g) + NH_3(g) \quad (1)$$

and elimination of HCl

$$AlCl_3NH_3(g) \rightleftarrows Cl_2AlNH_2(g) + HCl(g) \quad (2)$$

The thermal dissociation of the $AlCl_3NH_3$ adduct has been studied by unsaturated vapor pressure measurements. Dissociation was found to be reversible, and the thermodynamic properties of the process (eq 1) were obtained.[13] The reversible character of this process (eq 1) suggests a low activation energy for the adduct formation. Indeed, it has been predicted theoretically that reaction of $Ga(CH_3)_3$ with AsH_3 yields the adduct $Ga(CH_3)_3AsH_3$ without an activation barrier.[14] Adduct formation causes pyramidalization and bond lengthening in the acceptor molecule. Geometrical changes of the donor molecule were found to be less pronounced.[15,16]

In contrast, the second process (eq 2) involves geometrical changes for both aluminum and nitrogen centers, and the activation barrier for the reverse reaction should be considerable. Therefore, Cl_2AlNH_2, if formed, is expected to follow the dissociation/association process rather than HCl addition. No experimental thermodynamic data for this process (eq 2) are known.

[⊗] Abstract published in *Advance ACS Abstracts,* May 1, 1997.

(1) Hashman, T. W.; Pratsinis, S. E. *J. Am. Ceram. Soc.* **1992**, *75*, 920.
(2) Lee, W. Y.; Lackey, W. L.; Agrawal, P. K. *J. Am. Ceram. Soc.* **1991**, *74*, 1821.
(3) Chu, T. L.; Kelm, R. W. *J. Electrochem. Soc.* **1975**, *122*, 995.
(4) Jiang, Z.; Interrante, L. V. *Chem. Mater.* **1990**, *2*, 439.
(5) Sauls, F. C.; Interrante, L. V. *Coord. Chem. Rev.* **1993**, *128*, 193.
(6) Sauls, F. C.; Interrante, L. V.; Jiang, Z. *Inorg. Chem.* **1990**, *29*, 2989.
(7) Sauls, F. C.; Hurley, W. J.; Interrante, L. V.; Marchetti, P. S.; Maciel, G. E. *Chem. Mater.* **1995**, *7*, 1361.
(8) Kim, H. J.; Egashira, Y.; Komiyama, H. *Appl. Phys. Lett.* **1991**, *59*, 2521.
(9) Egashira, Y.; Kim, H. J.; Komiyama, H. *J. Am. Ceram. Soc.* **1994**, *77*, 2009.
(10) Kimura, I.; Hotta, N.; Nukui, H.; Saito, N.; Yasukawa, S. *J. Mater. Sci. Lett.* **1988**, *7*, 66.
(11) Kimura, I.; Hotta, N.; Nukui, H.; Saito, N.; Yasukawa, S. *J. Mater. Sci.* **1989**, *24*, 4076.
(12) Pauleau, Y.; Bouteville, A.; Hantzpergue, J. J.; Remy, J. C. *J. Electrochem. Soc.* **1980**, *127*, 1532.
(13) Suvorov, A. V. Ph.D. Thesis, Leningrad State University, 1977.
(14) Graves, R. M.; Scuseria, G. E. *J. Chem. Phys.* **1992**, *96*, 3723.
(15) Hargittai, M.; Hargittai, I. *The Molecular Geometries of Coordination Compounds in the Vapor Phase*; Elsevier: Amsterdam, 1977.
(16) *Stereochemical Applications of Gas-Phase Electron Diffraction. Part B. Structural Information for Selected Classes of Compounds*; Hargittai, I., Hargittai, M., Eds.; VCH Publishers: New York, 1988.

S0002-7863(96)04163-7 CCC: $14.00

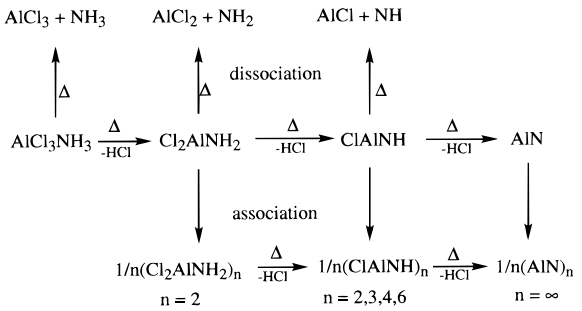

Figure 1. Scheme of CVD of AlN.

Similar to $AlCl_3NH_3$, there are two different channels for the decomposition process of Cl_2AlNH_2: Al−N bond breaking with formation of the $AlCl_2$ and NH_2 radicals and HCl detachment which leads to ClAlNH. Finally, decomposition of ClAlNH could result in AlN and HCl formation, with subsequent deposition of AlN films, or dissociation to AlCl and NH (Figure 1).

However, cluster formation in the gas phase indicates that complex chemical aggregates are present under the experimental conditions. $(Cl_2AlNH_2)_n$ and $(ClAlNH)_n$ associates (Figure 1) may be possible precursors of AlN cluster formation. Association of organoaluminum compounds is well-known. Amino- and iminoalanes can be produced by reaction of substituted alanes with primary amines according to the following scheme:

$$AlR_3 + NH_2R' \rightarrow {}^1/_n(R_2AlNHR')_n \rightarrow {}^1/_m(RAlNR')_m$$
aminoalane iminoalane

The chemistry of these compounds has recently been reviewed.[17,18] Both amino- and iminoalanes associate in solution and in the solid phase; however, the degree of association is different. Aminoalanes $(R_2AlNR_2)_n$ are known to exist in dimeric and trimeric forms in solution and in the solid phase,[18] and their dimer−trimer equilibrium was studied by NMR spectroscopy.[19] However, chloroalane derivatives are known to exist in the dimer form only. In fact, $(Cl_2AlNMe_2)_2$ is dimeric in the solid state,[20] in boiling benzene,[21] and in the gas phase.[22] While aminoalanes have been found to exist in monomeric, dimeric, and trimeric forms only,[17,23] iminoalanes tend to form polymer chains $(RAlNR')_n$[24] and clusters with $n = 4-8$, 10, 15, 16.[25,26] The structures of these compounds show the presence of Al_nN_n skeletons, and the degree of association was found to be determined by the size of the substituent R. More bulky substituents allow a lower degree of association. Iminoalanes with $n = 2$ have been synthesized very recently.[27−29]

All of these results suggest a high tendency to polymerization for sterically open ClAlNH species. To our knowledge, no small aggregates of $(ClAlNH)_n$ with $n = 1-4$, 6 have been isolated, due to the high tendency to polymerization. Formation of $(ClAlNCH_3)_n$ polymers was mentioned as early as 1960.[30] Reaction of *B*-trichloroborazine $(ClBNH)_3$ with $Al(C_2H_5)_3$ in *n*-dodecane leads to the evolution of $B(C_2H_5)_3$ gas and a solid residue of $(ClAlNH)_n$.[31] Thermolysis of $(Cl_2AlNHSiMe_3)_2$ at 170−200 °C results in formation of polymeric $(ClAlNH)_n$ and evolution of Me_3SiCl.[32] In turn, it was claimed[33] that pyrolysis of $(ClAlNH)_n$ in vacuum or ammonia at 700 °C yields crystalline AlN. In contrast, the boron analog *B*-trichloroborazine ($n = 3$) is known to be stable, and its pyrolysis at 1500 °C gave pure boron nitride.[34] Chlorine containing cages $(ClAlNR)_n$ with nonhydrogen ligands R have been characterized for $n = 4$, R = *i*-Pr, *t*-Bu[35−37] and for $n = 6$, R = *i*-Pr.[35] For the latter compound structural information is also available.[38]

Considering the CVD process, formation of oligomers in the gas phase is unfavorable due to the entropy factor; however, these reactions may be energetically favorable. Recent *ab initio* calculations of the model compounds $(H_2AlNH_2)_2$, $(HAlNH)_2$, and $(HAlNH)_4$ show that the energy of hydrogen elimination for the process $2(H_2AlNH_2)_2 \rightleftarrows (HAlNH)_4 + 4H_2$ is −114 kJ/mol at the SCF/DZP level of theory.[39] Therefore, despite the high temperatures during the experimental CVD process, oligomers can be formed in the gas phase.

In the present work, we studied the process of HCl elimination from $AlCl_3NH_3$ and the gas phase polymerization of intermediates (Figure 1). We present structures and energies for the $(Cl_2AlNH_2)_n$ $n = 1$, 2 and $(ClAlNH)_n$ $n = 1-4$, 6 compounds. Harmonic vibrational frequencies for these compounds are given as Supporting Information. Thermodynamic properties of the major processes in the gas phase are discussed as well.

Computational Details

All computations were performed using the *Gaussian* 94[40] program package. The full Dunning−Huzinaga double-ζ plus polarization basis set[41] was used throughout. Self-consistent field (SCF), second-order Møller−Plesset perturbation theory (MP2) and density functional methods (DFT) were used in this investigation. The three-parameter exchange functional of Becke[42] with the correlation functional of Lee, Yang, and Parr[43] (B3LYP) was used for the DFT studies. Geometries

(17) *Chemistry of Aluminium, Gallium, Indium, and Thallium*.; Downs, A. J., Ed.; Chapman & Hall: New York, 1993.
(18) *Coordination Chemistry of Aluminium*; Robinson, G. H., Ed.; VCH Publishers: New York, 1993.
(19) Sauls, F. C.; Czekaj, C. L.; Interante, L. V. *Inorg. Chem.* **1990**, *29*, 4688.
(20) Ahmed, v. A.; Schwarz, W.; Hess, H. *Acta Crystallogr.* **1977**, *B33*, 3574.
(21) Ruff, J. K.; Hawthorne, M. F. *J. Am. Chem. Soc.* **1960**, *82*, 1798.
(22) Ehrlich, R. *Inorg. Chem.* **1970**, *9*, 146.
(23) Petrie, M. A.; Ruhland-Senge, K.; Power, P. P. *Inorg. Chem.* **1993**, *32*, 1135.
(24) Jensen, J. A. In *Inorganic and Organometallic Polymers II. Advanced Materials and Intermediates*; Wilson-Nelson, W., Allcock, H. R., Wynne, K. J., Eds.; American Chemical Society: Washington, DC, 1994; p 427.
(25) Veith, M. *Chem. Rev.* **1990**, *90*, 3.
(26) Cesari, M.; Cucinella, S. In *The Chemistry of Inorganic Homo- and Heterocycles*; Haiduc, I., Sowerby, D. B.,, Eds.; Academic Press: London, 1987; Vol. 1, p 167.
(27) Schulz, S.; Hamig, L.; Herbst-Irmer, R.; Roesky, H. W.; Sheldrick, G. M. *Angew. Chem., Int. Ed. Engl.* **1994**, *33*, 969.
(28) Wehmschulte, R. J.; Power, P. P. *J. Am. Chem. Soc.* **1996**, *118*, 791.
(29) Fisher, J. D.; Shapiro, P. J.; Yap, G. P. A.; Rheingold, A. L. *Inorg. Chem.* **1996**, *35*, 271.
(30) Laubengayer, A. W.; Smith, J. D.; Ehrlich, G. G. *J. Am. Chem. Soc.* **1960**, *83*, 542.
(31) Woods, W. G.; McCloskey, A. L. *Inorg. Chem.* **1963**, *2*, 861.
(32) Becke-Goering, M.; Krill, H. *Chem. Ber.* **1961**, *94*, 1059.
(33) Schleich, D. M. U.S. Pat. 4,767,607, Aug 30, 1988.
(34) Haiduc, I. *The Chemistry of Inorganic Ring Systems*; Wiley: London, 1970.
(35) Cucinella, S; Salvatory, T.; Busetto, C.; Mazzei, A. *J. Organomet. Chem.* **1976**, *108*, 13.
(36) Busetto, C; Cesari, M.; Cucinella, S.; Salvatory, T. *J. Organomet. Chem.* **1977**, *132*, 339.
(37) Noth, H.; Wolfgardt, P. Z. *Naturforsch.* **1976**, *31b*, 697.
(38) Del Piero, G.; Perego, G.; Cucinella, S.; Cesari, M. C.; Mazzei, A. *J. Organomet. Chem.* **1977**, *136*, 13.
(39) Davy, R. D.; Schaefer, H. F. Submitted.
(40) *Gaussian 94*; Frisch, M. J.; Trucks, G. W.; Schlegel, H. B.; Gill, P. M. W.; Johnson, B. G.; Robb, M. A.; Cheeseman, J. R.; Keith, T.; Petersson, G. A.; Montgomery, J. A.; Raghavachari, K.; Al-Laham, M. A.; Zakrzewski, V. G.; Ortiz, J. V.; Foresman, J. B.; Cioslowski, J.; Stefanov, B. B.; Nanayakkara, A.; Challacombe, M.; Peng, C. Y.; Ayala, P. Y.; Chen, W.; Wong, M. W.; Andres, J. L.; Replogle, E. S.; Gomperts, R.; Martin, R. L.; Fox, D. J.; Binkley, J. S.; Defrees, D. J.; Baker, J.; Stewart, J. P.; Head-Gordon, M.; Gonzalez, C.; Pople, J. A.; Gaussian, Inc.: Pittsburgh, PA, 1995.
(41) Dunning, T.H.; Hay, P. J. *Modern Theoretical Chemistry*; Plenum: New York, 1976; Vol. 3.
(42) Becke, A. D. *J. Chem. Phys.* **1993**, *98*, 5648.

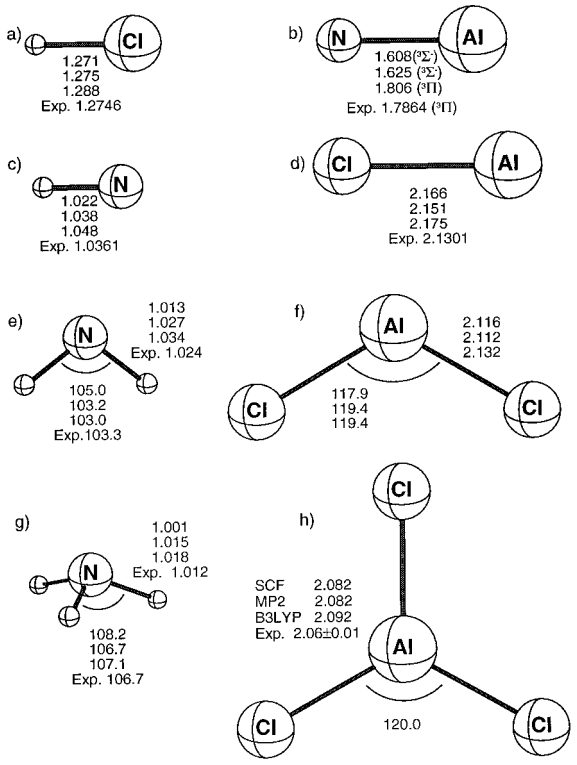

Figure 2. Geometries of NH_n and $AlCl_n$ species.

were fully optimized at each level of theory with subsequent vibrational analysis.

Results and Discussion

Geometries and Vibrational Frequencies. Geometries of investigated compounds are presented in Figures 2−10. Selected geometric parameters for all species are summarized in Table 6 together with experimental data and literature *ab initio* results. To facilitate the future experimental observation of intermediates we attached tables with harmonic vibrational frequencies and infrared intensities of Cl_2AlNH_2, ClAlNH, $(Cl_2AlNH_2)_2$, $(ClAlNH)_2$, $(ClAlNH)_3$, $(ClAlNH)_4$, and $(ClAlNH)_6$ as Supporting Information.

A. Donor and Acceptor Molecules. HCl, AlN. The geometries of HCl and AlN are given in Figure 2a and b, respectively. The calculated H−Cl distance is in good agreement with experiment.[44] AlN has previously been studied by complete active space SCF (CASSCF) and multireference configuration interaction methods.[45] In contrast to the CASSCF method, MRCI including the Davidson correction favors the $^3\Pi$ over the $^3\Sigma$ state. However, the energy difference[45] is only a few hundred reciprocal centimeters. Our predictions give a $^3\Sigma^-$ ground state for AlN at the SCF and MP2 levels of theory, but the hybrid Hartree−Fock/DFT method correctly gives the $^3\Pi$ state as the ground state. It should be noted that the B3LYP $^3\Pi$ frequency (734 cm^{-1}) is close to the experimental value of $\omega_e = 747$ cm^{-1} for AlN. SCF and MP2 give $^3\Sigma^-$ vibrational frequencies of 1183 and 1406 cm^{-1}, respectively, very different from the experimental $^3\Pi$ result. For AlN, our results at all levels of theory show that the closed-shell $^1\Sigma^+$ state lies much higher than $^3\Sigma^-$, in agreement with experiment.[45]

NH_n species and aluminum halides have been the subject of numerous experimental and *ab initio* investigations. Since the primary goal of this work is to identify the complex species in the CVD process, we will discuss the structures and vibrational frequencies of the NH_n and $AlCl_n$ species only briefly.

NH_n Species ($n = 1-3$). Geometric parameters for NH_3, NH_2, and NH are presented in Figure 2g, e, and c, respectively, and vibrational frequencies in Table 1. The theoretical structural data for C_{3v} NH_3 are in good agreement with experiment.[44] All methods overestimate the vibrational frequencies, and the B3LYP method gives results closer to experiment than SCF and MP2. The NH_2 radical is correctly found to have a $^2B_1$ ground state and C_{2v} symmetry. The N−H distance is slightly increased compared to ammonia, and the H−N−H angle is decreased by about 3−4°. NH has its well-known $^3\Sigma^-$ ground state with $C_{\infty v}$ symmetry. The N−H distance is longer compared to NH_2 and NH_3. The increasing N−H distance and decreasing vibrational N−H stretching mode suggests that the strength of N−H bond decreases in the order $NH_3 > NH_2 > NH$. In fact, the three experimental bond dissociation energies D_o are $(NH_2-H) = 448$, $(NH-H) = 399$, and $(N-H) = 310$ kJ mol^{-1}.[44,46]

$AlCl_n$ ($n = 1-3$). Geometries of $AlCl_3$, $AlCl_2$, and AlCl are given in Figure 2h, f, and d, respectively, and the corresponding vibrational frequencies are given in Table 2. In a recent study, Hassanzadeh *et al*. using DFT mentioned that the Al−Cl bond lengths for $AlCl_3$ are slightly inequivalent.[47] In contrast, we obtain a trigonal planar $AlCl_3$ molecule (D_{3h} symmetry) at all levels of theory. The theoretical Al−Cl distance is 0.02−0.03 Å longer than reported experimentally.[48] The B3LYP method gives better agreement with the experimental vibrational frequencies[49] than do SCF and MP2. The ground state of the $AlCl_2$ radical was found to be of $^2A_1$ symmetry in C_{2v} point group. The Al−Cl distance is longer than for $AlCl_3$ by 0.03−0.04 Å. The Cl−Al−Cl angle was predicted to be slightly decreased, but at the MP2 and B3LYP levels of theory its value is 119.4°, very close to the trigonal 120° found for $AlCl_3$. There are apparently no experimental geometrical data available for $AlCl_2$. The theoretical vibrational frequencies are in good agreement with experimental results obtained in solid argon matrices.[47,50] AlCl has a $^1\Sigma^+$ electronic ground state. The Al−Cl distance is further increased compared to $AlCl_2$. The theoretical stretching frequency at the B3LYP level (Table 2) falls between the IR matrix isolation result[47,50] and the gas phase result.[46]

B. Adducts. $AlCl_3NH_3$. The geometry of $AlCl_3NH_3$ is presented in Figure 3. The molecule has the expected C_{3v} symmetry with a staggered orientation of the fragments. Geometrical parameters are in good agreement with gas phase electron diffraction data[51] and previous *ab initio* results.[52−54] The Al−Cl and N−H bond lengths in the adduct are increased by 0.043 and 0.005 Å, respectively, compared to free $AlCl_3$ and NH_3. The $AlCl_3$ fragment in the adduct is distorted about

(43) Lee, C.; Yang, W.; Parr, R. G. *Phys. Rev. B* **1988**, *37*, 785.
(44) *Handbook of Chemistry and Physics*, 75th ed.; Lide, D. R., Ed.; CRC Press: Boca Raton, FL, 1995.
(45) Langhoff, S. R.; Bauschlicher, C. W.; Petterson, L. G. M. *J. Chem. Phys.* **1988**, *89*, 7354.
(46) Huber, K. P.; Herzberg, G. *Constants of Diatomic Molecules*; Van Nostrand Reinhold Co.: New York, 1979.
(47) Hassanzadeh, P.; Citra, A.; Andrews, L.; Neurock, M. *J. Phys. Chem.* **1996**, *100*, 7317 and references therein.
(48) Zasorin, E. Z.; Rambidi, N. G. *Zh. Struct. Khim.* **1967**, *8*, 391.
(49) Tomita, T.; Sjogren, C. E.; Klaeboe, P.; Papatheodorou, G. N.; Rytter, E. *J. Raman Spectrosc.* **1983**, *14*, 4515.
(50) Olah, G. A.; Farooq, O.; Morteza, S.; Farnia, F.; Bruce, M. R.; Clouet, F. L.; Morton, P. R.; Prakash, G. K. S.; Stevens, R. C.; Bau, R.; Lammertsma, K.; Suzer, S.; Andrews, L. *J. Am. Chem. Soc.* **1988**, *110*, 3231.
(51) Hargittai, M.; Hargittai, I.; Spiridonov, V. P.; Pelissier, M.; Labarre, J. F. *J. Mol. Struct.* **1975**, *24*, 27.
(52) Connolly, J. W.; Dudis, D. S. *Macromolecules* **1994**, *27*, 1432.
(53) Branchadell, V.; Sbai, A.; Oliva, A. *J. Phys. Chem.* **1995**, *99*, 6472.
(54) Chey, J.; Choe, H. S.; Chook, Y.-M.; Jensen, E.; Seida, P. R.; Fancl, M. M. *Organometallics* **1990**, *9*, 2430.

Table 1. Harmonic Vibrational Frequencies (cm^{-1}) and Infrared Intensities in Parentheses (km mol^{-1}) for NH_n Species

compound	mode	SCF	MP2	B3LYP	experiment[a]
NH_3	A_1 ν_1 NH sym stretch	3724 (0.4)	3568 (0.004)	3497 (0.2)	3337
	A_1 ν_2 sym def	1114 (235)	1099 (188)	1038 (192)	950
	E ν_3 NH antisym stretch	3871 (3)	3736 (2)	3637 (0.8)	3444
	E ν_4 antisym def	1803 (25)	1706 (19)	1679 (21)	1627
NH_2	A_1 ν_1 NH sym stretch	3630 (4)	3489 (7)	3361 (13)	3219
	A_1 ν_2 bend	1646 (37)	1567 (24)	1534 (20)	1497
	B_2 ν_3 NH antisym stretch	3738 (2)	3616 (3)	3469 (6)	3301
NH $^3\Sigma$	Σ_g ν_1 NH stretch	3526 (23)	3420 (30)	3258 (35)	

[a] Experimental data from ref 44.

Table 2. Harmonic Vibrational Frequencies (cm^{-1}) and Infrared Intensities in Parentheses (km mol^{-1}) for $AlCl_n$ Species

compound	mode	SCF	MP2	B3LYP	experiment
$AlCl_3$	A_1' ν_1 AlCl sym stretch	399 (0)	395 (0)	378 (0)	375[a]
	A_2'' ν_2 sym def	218 (58)	214 (45)	202 (38)	214[a]
	E′ ν_3 AlCl antisym stretch	642 (215)	643 (184)	617 (172)	616[a]
	E′ ν_4 antisym stretch	154 (12)	151 (10)	145 (8)	151[a]
$AlCl_2$	A_1 ν_1 AlCl sym stretch	478 (67)	474 (52)	442 (45)	461[b]
	A_1 ν_2 bend	161 (14)	155 (11)	143 (8)	
	B_2 ν_3 AlCl antisym stretch	588 (199)	599 (170)	558 (155)	564[b,c]
AlCl $^1\Sigma$	Σ_g ν_1 AlCl sym stretch	479 (151)	497 (122)	466 (115)	455,[b,c] 481[d]

[a] Reference 49. [b] Reference 47. [c] Reference 50. [d] Reference 46.

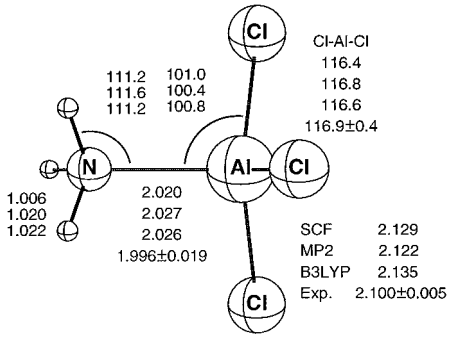

Figure 3. Geometry of $AlCl_3NH_3$ adduct.

Table 3. Harmonic Vibrational Frequencies (cm^{-1}) and Infrared Intensities in Parentheses (km mol^{-1}) for $AlCl_3NH_3$

mode	SCF	B3LYP	experiment[a]
	A_1		
ν_1 NH sym stretch	3680 (37)	3464 (25)	3302 m
ν_2 NH_3 sym def	1439 (265)	1317 (216)	1263 vs
ν_3 AlN stretch	490 (63)	473 (47)	474 s
ν_4 AlCl sym stretch	388 (10)	369 (8)	378 (w)
ν_5 $AlCl_3$ sym def	204 (47)	192 (37)	200 s
	A_2		
ν_6 AlN torsion	61 (0)	47 (0)	276
	E		
ν_7 NH antisym stretch	3807 (70)	3583 (48)	3395 m
ν_8 NH_3 antisym def	1779 (36)	1651 (30)	1614 w
ν_9 NH_3 rock	776 (136)	727 (132)	702 vs
ν_{10} AlCl antisym stretch	562 (131)	542 (96)	536 vs
ν_{11} $AlCl_3$ rock	167 (0.5)	155 (0.1)	186 s
ν_{12} $AlCl_3$ antisym def	127 (11)	118 (10)	123 m

[a] Gas phase IR spectroscopy data from ref. 55.

10° from planarity, leading to a decrease of the Cl−Al−Cl angle from 120° to 116.6°.

Theoretical vibrational frequencies for $AlCl_3NH_3$ are presented in Table 3 together with experimental gas phase IR data.[55] Although our predictions for the torsion frequency are in good agreement with earlier computational work (74 cm^{-1} at SCF/6-31G* level of theory),[52] there is a remarkable deviation from the experimental value of 276 cm^{-1} obtained by Sjogren and Rytter.[55] As the torsion mode has A_2 symmetry and is inactive in both the IR and Raman spectra, the reported experimental value was derived from a weak combination band. However, upon analysis of torsion frequencies of substituted ethanes, Papatheodorou *et al.*[56] estimated an upper limit of 225 cm^{-1} for the torsion. These authors concluded that the actual torsion mode could lie anywhere between 100 and 225 cm^{-1}.[56] Therefore, the experimental value of 276 cm^{-1} seems to be too high. Our predicted frequencies (61 and 47 cm^{-1} at the SCF and B3LYP levels of theory, respectively) are of the same order as the experimental torsion frequencies for CCl_3CCl_3 (61 cm^{-1}) and CBr_3CBr_3 (51 cm^{-1}).[57]

A small value of the torsion mode frequency indicates that the barrier for internal rotation is low. Sjogren and Rytter[55] estimated the rotational barrier using their 276 cm^{-1} torsion mode and the experimental geometry to be 20 kJ mol^{-1}. In order to obtain the value of the internal rotation barrier, we investigated the $AlCl_3NH_3$ eclipsed conformation, which is the transition state for rotation about the Al−N bond. However, the energy difference between these conformers is very small (0.6 kJ mol^{-1} at the B3LYP level and at least 30 times less than that derived from the spectra) in agreement with early *ab initio* results (2.0 kJ mol^{-1} with the SCF/STO-3G* method). Low barriers are also obtained for ammonia alane[58] (3.1 kJ mol^{-1}) and trimethylammonia alane[59] (10.9 kJ mol^{-1}) at the coupled cluster level of theory with single and double excitations (CCSD/DZP). The latter rotational barrier is higher due to the steric repulsion of methyl substituents. These data suggest, in contrast to the experiments mentioned above,[55] that rotational barriers for R_3AlNH_3 adducts are quite small ($\leq$3 kJ mol^{-1}). After including the zero-point vibrational energy (ZPVE), the eclipsed conformer is slightly lower lying than the staggered. A weak bonding interaction between eclipsed H and Cl might stabilize the eclipsed conformer. A similar interaction involving H···Br has been observed for $Cy_2GaBrNH_2Ph$ (Cy = cyclohexene) in the solid phase.[60] The existence of H···Cl intramolecular interactions might facilitate the elimination of HCl.

(55) Sjogren, C. E.; Rytter, E. *Spectrochim. Acta* **1985**, *41A, N11*, 1277.
(56) Papatheodorou, G. N.; Curtiss, L. A.; Maroni, V. A. *J. Chem. Phys.* **1983**, *78*, 3303.
(57) Shimanouchi, T. *Tables of Molecular Vibration Frequencies, Part 2*; National Bureau of Standards: Washington, DC, 1967.
(58) Marsh, G. M. B.; Hamilton, T. P.; Xie, Y.; Schaefer, H. F. *J. Chem. Phys.* **1992**, *96*, 5310.
(59) Marsh, G. M. B.; Schaefer, H. F. *J. Phys. Chem.* **1995**, *99*, 195.

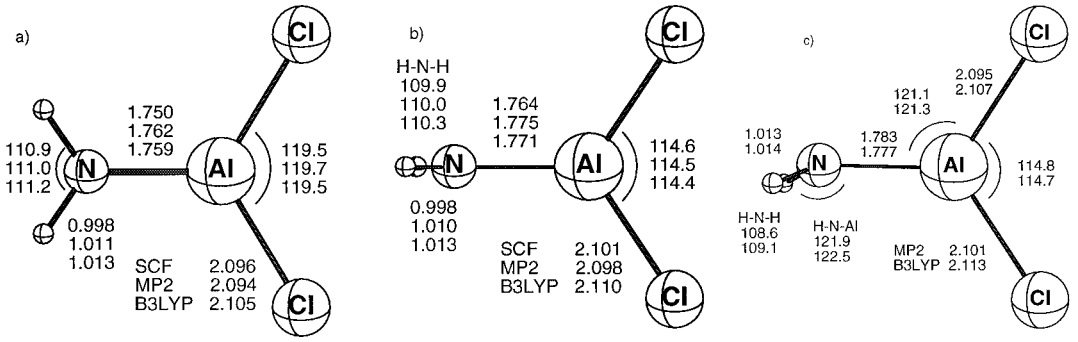

Figure 4. Geometries of Cl_2AlNH_2 conformers.

Table 4. Calculated Al−N Distances (Å) for Ground and Transition States of R_2AlNH_2 Compounds and Rotational Barrier (kJ mol^{-1})

R	Al−N	Δ_1[a]	percent	Al−N TS	Δ_2[b]	percent	E_{rot}	method
CH_3	1.790	−0.316	15.0	1.823	0.033	1.8	40.7	MP2/6-31G* [e]
H	1.772	−0.309	14.7	1.791[c]	0.019[c]	1.1[c]	44.8[c]	CCSD/DZP[c]
Cl	1.759	−0.267	13.2	1.777	0.018	1.0	33.6	B3LYP/DZP
1, **2**[d]	1.78−1.83						38−42	exp[f]

[a] Difference of Al−N bond length between R_2AlNH_2 and R_3AlNH_3. [b] Difference of Al−N bond length between transition state and equilibrium geometry for R_2AlNH_2 compounds. [c] Data for staggered conformation from ref 64. [d] See text for definitions of the experimentally synthesized compounds **1** and **2**. [e] Reference 61. [f] Reference 23.

$AlCl_2NH_2$. In monomeric aminoalanes aluminum and nitrogen are 3-coordinated, leading to polymerization with formation of 4-coordinated dimer and trimer forms.[17] Only a few monomer aminoalanes have been structurally characterized so far; all of them have bulky ligands both on the ammonia and aluminum centers.[23] Recently, matrix isolation and *ab initio* MP2 results for $(CH_3)_2AlNH_2$ have been reported.[61] The prototypical hydrogen analog H_2AlNH_2 has been studied using SCF/6-31G*,[62] GVB/DZP,[63] and more recently, CCSD/TZ2P methods.[64]

$AlCl_2NH_2$ is a planar molecule with C_{2v} symmetry. Geometric parameters are presented in Figure 4a. The calculated Al−N bond length (1.759 Å B3LYP) is shorter than the experimental values (1.78−1.89 Å) for the $R_2AlNR'_2$ monomers synthesized by Power and co-workers.[23] However, none of the synthesized monomers are planar, and the experimental dihedral angles between the R_2Al and NR'_2 planes are in the range between 5.5° and 87.7°. This distortion from planarity results from steric interactions of the bulky substituents. Two compounds with small dihedral angles, 5.5° for (2,4,6-*i*-$Pr_3C_6H_2)_2$-AlNH(2,6-*i*-$Pr_2C_6H_3$) (**1**) and 16.1° for (*t*-$Bu)_2$AlN(2,6-*i*-$Pr_2C_6H_3$)-$SiPh_3$ (**2**) have Al−N distances of 1.784 and 1.834 Å, respectively. For H_2AlNH_2[64] and Me_2AlNH_2,[61] planar structures were obtained theoretically, in good agreement with matrix isolation IR data for the latter compound.

The Cl−Al−Cl angle in $AlCl_2NH_2$ is 119.6°, which is close to the 119.4° angle we predict for the $AlCl_2$ radical. The Al−Cl and N−H bond lengths in $AlCl_2NH_2$ are considerably shorter than in the free $AlCl_2$ and NH_2 radicals, in contrast to $AlCl_3NH_3$, where the Al−Cl and N−H bond distances increase compared to free $AlCl_3$ and NH_3. This indicates that adduct formation stabilizes both the $AlCl_2$ and NH_2 fragments.

The experimental value for the Al−N stretching mode in a monomeric amidoalane is 840 cm^{-1} for $Al[N(SiMe_3)_2]_3$.[65] Power *et al*. observed a strong band at 800 ± 10 cm^{-1} for all his synthesized monomer aminoalanes, which was ascribed to the Al−N stretching mode.[23] The theoretical values are somewhat higher than experiment: 865, 863, and 876 cm^{-1} for Cl_2AlNH_2, Me_2AlNH_2, and H_2AlNH_2, respectively. The torsion frequency is much higher than that for $AlCl_3NH_3$, indicating a higher barrier for internal rotation, which might be ascribed to π-bonding.

In order to investigate the π-bonding contribution to the strength of the Al−N bond, we studied the staggered conformer of $AlCl_2NH_2$ (Figure 4b). At the SCF level, the C_{2v} form is a transition state for internal rotation. However, at the MP2 and B3LYP levels of theory this was found to be a stationary point with Hessian index two, with one imaginary frequency corresponding to the pyramidalization of the nitrogen center. Thus, the transition state for internal rotation has C_s symmetry at the MP2 and B3LYP levels of theory (Figure 4c). Theoretical values for the rotation barrier are 32.8, 35.9, and 33.6 kJ mol^{-1} at the SCF, MP2, and B3LYP levels, respectively (including ZPVE correction). Our results may be compared to the experimental results of Power (38−42 kJ mol^{-1}) and previous calculations for R_2AlNH_2 compounds (46.8[62] and 44.8[64] kJ mol^{-1} for R = H and 40.7[61] kJ mol^{-1} for R = CH_3). Compared to R_3AlNH_3 adducts, the Al−N distance in R_2AlNH_2 compounds decreases significantly (by 13−15%), indicating the probability of double bond character (Table 4). For the transition state we observe a 1.0−1.8% increase of the Al−N bond length, which indicates that the π-contribution is small. The highest π-contribution is found for CH_3 substituents and the lowest for Cl, using the bond lengthening and the rotational barrier as criteria. Cl_2AlNH_2 has a lower rotational barrier than the H and CH_3 derivatives. Despite the weaker π-interactions, the Al-N distance in R_2AlNH_2 follows the same order as for the R_3AlNH_3 adducts: CH_3 > H > Cl, indicating stronger bonding in Cl_2AlNH_2. Thus, the enhanced bond strength is primarily due to electrostatic interactions between aluminum and nitrogen. Charge separation is facilitated by electron transfer to the electronegative chlorine atoms. Atomic charges from Mulliken population analyses are +0.94 on Al and −0.82 on N in Cl_2AlNH_2 and +0.86 and −0.72 in Cl_3AlNH_3. Higher charge separation in Cl_2AlNH_2 leads to the observed bond

(60) Atwood, D. A.; Cowley, A. H. *J. Organomet. Chem.* **1992**, *430*, C29.
(61) Müller, J. *J. Am. Chem. Soc.* **1996**, *118*, 6370.
(62) Reed, A. E.; Schleyer, P. v. R. *Inorg. Chem.* **1988**, *27*, 3969.
(63) Lynam, M. M.; Interrante, L. V.; Patterson, C. H.; Messmer, R. P. *Inorg. Chem.* **1991**, *30*, 1918.
(64) Davy, R. D.; Jaffrey, K. L. *J. Phys. Chem.* **1994**, *98*, 8930.
(65) Burger, H.; Cichen, J.; Goetze, U.; Wannagat, U.; Wismar, H. J. *J. Organomet. Chem.* **1971**, *33*, 1.

Table 5. Relative Energies of ClAlNH Isomers Including Zero-Point Vibrational Energies (kJ mol^{-1})

	SCF	MP2	B3LYP
singlet C_s	0	0	0
singlet $C_{\infty v}$	0	12.8	12.4
triplet C_1	−44.6	128.0	88.8
triplet C_s	−40.8	135.2	100.9

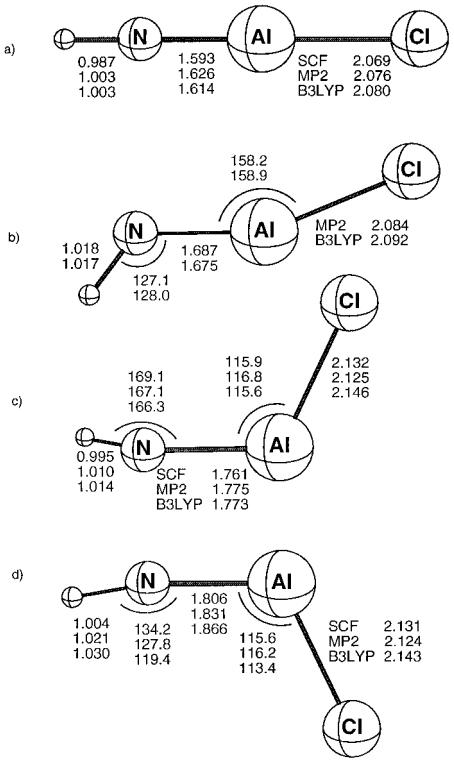

Figure 5. Geometries of ClAlNH conformers.

shortening. We conclude, that the electronegativity of the ligands on the Al center plays the key role in the bonding in the R_2AlNH_2 and R_3AlNH_3 systems by facilitating donation of electrons from nitrogen to aluminum and increasing charge separation on the Al and N centers.

ClAlNH. For the molecular system with one Al, two H, and one N atom, the $AlNH_2$ isomer has been found to be preferable to HAlNH[64] due to the stronger N−H bond compared to Al−H. For ClAlNH, we expect the reverse situation, because the Al−Cl bond is stronger than the N−Cl bond,[44] making ClAlNH the best possible ligand arrangement.

For ClAlNH we consider two possible structures: a singlet state with an Al−N double bond and a triplet structure with an Al−N single bond (see Table 5). The singlet linear structure ($C_{\infty v}$ symmetry) was first optimized using the SCF method. However, this linear structure was shown to be a transition state both at the MP2 and B3LYP levels of theory. A bent planar form (C_s symmetry) was eventually found to be the ground state geometry of ClAlNH. Geometries for both the linear and the C_s structures are given in the Figure 5a,b. The linear molecule has a very short Al−N distance: 0.4 Å less than in $AlCl_3NH_3$. Similarly, the Al−Cl distance is shorter than for $AlCl_3$. For the triplet state the planar structure is a transition state with respect to N−H distortion. The triplet equilibrium geometry is asymmetric at all levels of theory. Geometries of the transition state (C_s symmetry) and triplet ground state of ClAlNH are given in Figure 5c and d, respectively. In the triplet, the Al−N bond is 0.19 Å longer than in the singlet. In general, Al−N distances in singlet and triplet ClAlNH are similar to those in the respective AlN states. At the SCF level the triplet lies 45 kJ mol^{-1} lower than the singlet; however, at the MP2 and B3LYP levels the singlet structure was found to be more stable by 128 and 89 kJ mol^{-1}, respectively (all data are given with ZPVE corrections).

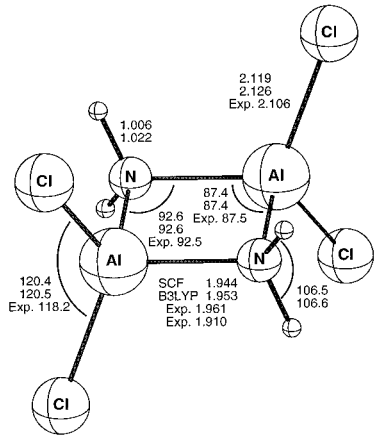

Figure 6. Geometry of $(Cl_2AlNH_2)_2$.

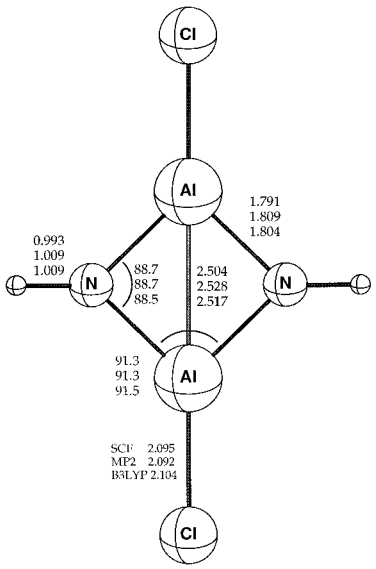

Figure 7. Geometry of $(ClAlNH)_2$.

C. Oligomers. $(Cl_2AlNH_2)_2$. The geometry of $(Cl_2AlNH_2)_2$ is given in Figure 6. In agreement with gas phase electron diffraction data for $(Cl_2AlNMe_2)_2$,[66] we find D_{2h} symmetry for $(Cl_2AlNH_2)_2$. It should be noted that in the solid state[20] the Al−Cl bonds are reported to be inequivalent (2.088 and 2.123 Å, compared to 2.106 Å in the gas phase), lowering the symmetry to C_{2h}, and the Al−N distance is decreased to 1.910 Å compared to 1.961 Å in the gas phase. Our results can be compared to recent *ab initio* work for the parent dimer $(H_2AlNH_2)_2$.[39] The Al−N distance for the Cl derivative is shorter than for the H derivative (1.944 and 1.961 Å, respectively, at the SCF level of theory), indicating the stronger bonding in $(Cl_2AlNH_2)_2$. The Al_2N_2 ring angles are in excellent agreement with experiment.[20] The Al−Al distance is quite short compared to the sum of the atomic radii of Al, but exclusively due to the geometric restrictions for the ring structure.

$(ClAlNH)_2$. The predicted geometry of $(ClAlNH)_2$ is presented in Figure 7. The structure incorporates a planar Al_2N_2 ring, in agreement with the hydride analog. As mentioned earlier, a low degree of association is not typical for iminoalanes,

(66) Bartke, T. C.; Haaland, A.; Novak, D. P. *Acta Chem. Scand.* **1975**, *A29*, 273.

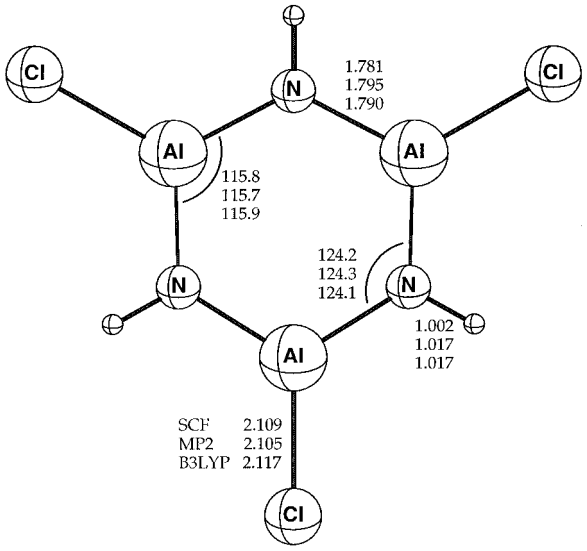

Figure 8. Geometry of $(ClAlNH)_3$.

and only three dimeric compounds have been synthesized so far,[27−29] two of them very recently. The first is Cp*{$(Me_3Si)_2N$}AlN(μ-AlCp*)(μ-Al{$N(SiMe_3)_2$})$NAlCp_2$* (Cp* = η^1-C_5Me_5) (**3**),[27] whose composition formally corresponds to the $[Cp^*AlN(SiMe_3)]_4$ cubane structure. The crystal structure for compound **3** is characterized by a nearly planar Al_2N_2 ring, and three out of four ring atoms preserve Al−N bonds outside the ring. This indicates that **3** is derived from the cubane structure by breaking its top layer, with subsequent rearrangement of the $SiMe_3$ and Cp* groups. The mean Al−N distance inside the ring was found to be 1.811(7) Å.[27] The second experimental structure $(Mes^*AlNPh)_2$ (Mes* = 2,4,6-(*t*-Bu)$_3C_6H_2$) (**4**) has a planar Al_2N_2 ring with equivalent Al−N distances 1.824(2) Å.[28] Both Al and N atoms have aryl substitutes. The third structure, $[(\eta^5\text{-}C_5H_5)AlN(2,6\text{-}i\text{-}Pr_2C_6H_3)]_2$ (**5**),[29] has a flat Al_2N_2 ring with η^5-coordination of the cyclopentadienyl rings and a perpendicular orientation for the bulky aryl groups. The mean Al−N distance in the ring is 1.804 Å.[29]

The theoretical Al−N bond length is in good agreement with the experimental structure **5**,[29] and slightly shorter than found in **3** and **4**.[27,28] There is a clear difference of Al−Al distances between 2.429 Å in **1**[23] and 2.607 Å in **4**.[28] The theoretical value of 2.517 Å falls in between these two and is close to the observed value 2.569 Å in **5**.[29] However, the short Al−Al distance does not imply the existence of an Al−Al bond. It rather arises from geometric factors. The N−Al−N and Al−N−Al angles are 90 ± 1.5° in **4**, **5**, and the model compounds, while for **3** they deviate by 5° from 90°. This difference is the result of the highly inequivalent substituents in **3**.

$(ClAlNH)_3$. The geometry of the aluminum analog of *B*-trichloroborazene, $(ClAlNH)_3$, is given in Figure 8. $(ClAlNH)_3$ is planar and has D_{3h} symmetry at all levels of theory. The only experimentally known trimeric iminoalane is $[MeAlN(2,6\text{-}i\text{-}Pr_2C_6H_3]_3$ (**6**), synthesized by Power and co-workers in 1988.[67] They report an Al−N bond length of 1.782(4) Å, which is in good agreement with our theoretical value of 1.790 Å. The carbon atoms bonded to Al and N in **6** are coplanar with the ring, in agreement with the *ab initio* planar structures for $(ClAlNH)_3$ and $(HAlNH)_3$.[48,68] For the latter, prismane and chair/boat conformers have been found to be higher in energy than the benzene-like structure.[68] Geometric parameters for different trimeric iminoalanes $(RAlNR')_3$ are summarized in Table 6.

$(ClAlNH)_4$. The geometry of the $(ClAlNH)_4$ cube (T_d symmetry) is presented in Figure 9. The $(ClAlNR)_4$ compounds (R = *i*-Pr, *t*-Bu) have been synthesized from the analogous hydride;[35−37] however, there is no structural data available. Our predicted Al−N bond length is in good agreement with experimental structures for $(RAlNR')_4$ compounds[69,70] and the theoretical value for $(HAlNH)_4$.[39] The Al−N−Al and N−Al−N angles deviate by no more than 0.5° from 90° for all experimental and theoretical structures. Waggoner and Power observed that the N−Al−N angle tends to be smaller than the Al−N−Al angle;[71] however, the difference was within the experimental error margin. Our computational results for $(ClAlNH)_4$ confirm this.

$(ClAlNH)_6$. The geometry of $(ClAlNH)_6$ is presented in Figure 10. The molecule has D_{3d} symmetry with highly inequivalent Al−N bond lengths in the Al_3N_3 (1.901 Å) and Al_2N_2 (1.967 Å) rings. This is in good agreement with the experimental structure for $(ClAlN\text{-}i\text{-}Pr)_6$: 1.906 Å (mean) and 1.955 Å, respectively.[38,72] $(ClAlN\text{-}i\text{-}Pr)_6$ was found to possess S_6 symmetry with slightly different distances inside the Al_3N_3 ring: 1.898 and 1.914 Å. The lowering of the symmetry from D_{3d} to S_6 is due to the isopropyl substituent on the nitrogen centers, resulting in a 3° difference between the theoretical and experimental angles inside the Al_3N_3 ring. Our predicted Al−Cl distance (2.123 Å B3LYP) is in excellent agreement with the experimental value (2.122 Å).[38]

General Remarks on Molecular Structures. The theoretical and experimental Al−N bond lengths and Al−N−Al, N−Al−N angles for the investigated compounds are summarized in Table 6. The shortest Al−N distance is found for 2-coordinated RAlNR′ compounds (mean 1.65 Å), while for 3-coordinated compounds the mean Al-N distance is 1.79 Å. The longest Al−N distance observed is for the 4-coordinated $R_3AlNR'_3$ adducts, with pure dative bonds. Increasing the number of Al/N neighbors results in decreasing the Al−N bond length to 1.96 Å in the 4-membered ring and 1.92 Å in the cube compounds. In general, the Al−N−Al and N−Al−N angles are close to 90° in the Al_2N_2 and Al_4N_4 skeleton structures, while significant differences are observed only with highly inequivalent bulky ligands. For Al_3N_3 and Al_6N_6 skeleton structures, the N−Al−N angles (mean 116°) is lower than Al−N−Al angle (mean 124°). The same is true for Al_4N_4 cube structures, but the difference in the N−Al−N and Al−N−Al angles is not as pronounced.

Trends in Vibrational Frequencies. We have found that the B3LYP method gives vibrational frequencies in good agreement with experiment for low vibrational frequencies and overestimates higher frequencies (Figure 11). Recently, experimental and BLYP and B3LYP values for the vibrational frequencies of different organic molecules have been compared and selective scaling procedures have been proposed.[73] It was found that B3LYP and BLYP slightly overestimate vibrational frequencies. However, all of the experimental frequencies used were above 500 cm^{-1}. Our data are in agreement with these results in this range, but the lower frequencies are mostly

(67) Waggoner, K. M.; Hope, H.; Power, P. P. *Angew. Chem., Int. Ed. Engl.* **1988**, *27*, 1699.
(68) Matsunaga, N.; Gordon, M. S. *J. Am. Chem. Soc.* **1994**, *116*, 11407.
(69) Del Piero, G.; Cesari, M.; Dozzi, G.; Mazzei, A. *J. Organomet. Chem.* **1977**, *129*, 281.
(70) McDonald, T. R. R.; McDonald, W. S. *Acta Crystallogr.* **1972**, *B28*, 1619.
(71) Waggoner, K. M.; Power, P. P. *J. Am. Chem. Soc.* **1991**, *113*, 3385.
(72) Cesari, M.; Perego, G.; Del Piero, G.; Cucinella, S.; Cernia, E. *J. Organomet. Chem.* **1974**, *78*, 203.
(73) Rauhut, G.; Pulay, P. *J. Phys. Chem.* **1995**, *99*, 3093.

Table 6. Theoretical and Experimental Geometries for 2-, 3-, and 4-Coordinated Aluminum−Nitrogen Compounds[a]

CN	type	compound	Al−N	N−Al−N	Al−N−Al	method	references
2	RAlNR′	HAlNH	1.633			CCSD/TZ2P	64
		ClAlNH	1.675			B3LYP/DZP	this work
3	$R_2AlNR'_2$	**1**	1.784			X-ray	23
		2	1.834			X-ray	23
		Me_2AlNH_2	1.790			MP2/6-31G*	61
		H_2AlNH_2	1.772			CCSD/TZ2P	64
		Cl_2AlNH_2	1.759			B3LYP/DZP	this work
3	$(RAlNR')_2$	**3**	1.811[b]	95.6	84.3	X-ray	27
		4	1.824	88.75	91.25	X-ray	28
		5	1.804[b]	89.2	90.8	X-ray	29
		$(HAlNH)_2$	1.803	90.8	89.2	CCSD/DZP	39
		$(ClAlNH)_2$	1.804	91.5	88.5	B3LYP/DZP	this work
3	$(RAlNR')_3$	**6**	1.782	115.3	124.7	X-ray	67
		$(HAlNH)_3$	1.791	114.7	125.3	SCF/6-31G*	48
			1.787	114.2	125.8	SCF/ECP	68
		$(ClAlNH)_3$	1.781	115.8	124.2	SCF/DZP	this work
			1.790	115.9	124.1	B3LYP/DZP	this work
4	$R_3AlNR'_3$	Me_3AlNH_3	2.106			MP2/6-31G*	61
		H_3AlNH_3	2.077			CCSD/DZP	58
		Cl_3AlNH_3	1.996			electron diffraction	51
			2.026			B3LYP/DZP	this work
4	$(R_2AlNR'_2)_2$	$(Cl_2AlNMe_2)_2$	1.961	87.5	92.5	electron diffraction	66
		$(Cl_2AlNMe_2)_2$	1.910	88.6	91.4	X-ray	20
		$(H_2AlNH_2)_2$	1.967	87.0	93.0	CCSD/DZP	39
		$(Cl_2AlNH_2)_2$	1.953	87.4	92.6	B3LYP/DZP	this work
4	$(RAlNR')_4$	(MeAlN-*i*-Pr)$_4$	1.923	89.6	90.4	X-ray	69
		(HAlN-*i*-Pr)$_4$	1.913	89.9	90.1	X-ray	69
		$(PhAlNPh)_4$	1.915	89.8	90.2	X-ray	70
		$(HAlNH)_4$	1.923	89.1	90.9	SCF/DZP	39
		$(ClAlNH)_4$	1.919	89.5	90.5	SCF/DZP	this work
		$(ClAlNH)_4$	1.932	89.4	90.6	B3LYP/DZP	this work
6[c]	$(RAlNR')_6$	(MeAlN-*i*-Pr)$_6$	1.898[b]	116.4	123.2	X-ray	38
			1.956	91.4	88.5		
		(HAlN-*i*-Pr)$_6$	1.917[b]	115.7	123.9	X-ray	72
			1.964	91.4	88.55		
		(ClAlN-*i*-Pr)$_6$	1.906[b]	117.7	122.0	X-ray	38
			1.955	91.85	88.1		
		$(ClAlNH)_6$	1.901	114.5	125.4	B3LYP/DZP	this work
			1.972	89.6	90.2		

[a] Bond lengths in angstroms; bond angles in degrees. [b] Mean value. [c] For all $(RAlNR')_6$ compounds, data in the first row refer to the Al_3N_3 ring, data in the second row to the Al_2N_2 ring.

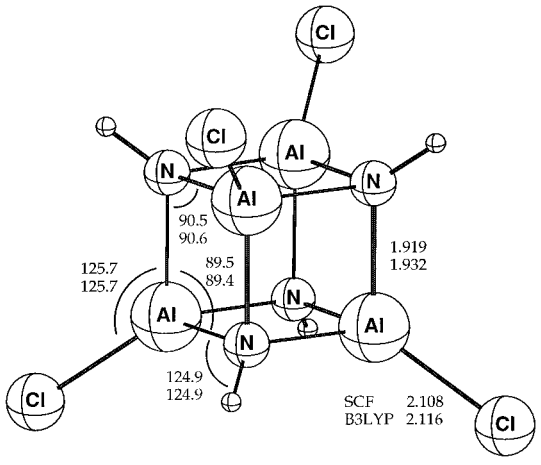

Figure 9. Geometry of $(ClAlNH)_4$.

underestimated. In order to scale the computed values, we propose that the observed and calculated frequencies are related through the following equation:

$$\nu_{obsd} = A\omega_{calcd} + B \qquad (3)$$

Using the B3LYP data as ω_{calcd} and the experimental data as ν_{obsd} for ammonia, NH_2, $AlCl_3$ and 11 (excluding torsion) frequencies of $AlCl_3NH_3$ (total of 22 frequencies), we obtained the following coefficients: $A = 0.9461$ and $B = 22.1$ cm^{-1} with correlation coefficient 0.9999. The good correlation suggests that our B3LYP vibrational frequencies for the molecules investigated are consistent. From the results shown, B3LYP slightly underestimates vibrational frequencies below 500 cm^{-1}. It would be interesting to test the performance of hybrid Hartree−Fock/DFT methods for predicting low vibrational frequencies for a wider range of compounds.

Conclusions: Thermodynamics. To test the performance of the methods used in the prediction of thermodynamic properties we have compared theoretical enthalpies of atomization, enthalpies of formation, and dissociation reaction enthalpies with experimental data, where available. These results are reported in Table 7. The SCF data represent poor agreement with experiment, the MP2 results are better, and the B3LYP data provide the best agreement. Thus, all thermodynamic analyses were performed using the B3LYP data. Gibbs energies for the different temperatures were obtained assuming the temperature independence of ΔH and ΔS. The theoretical standard enthalpies, entropies, and Gibbs energies for the different association and dissociation reactions are summarized in Table 8.

A. Stability of Cl_xAlNH_x ($x = 1-3$) Species. Theoretical results for the different channels of dissociation for Cl_xAlNH_x species are shown in Figure 12. Dissociation to components was found to be preferable to HCl detacment for all Cl_xAlNH_x compounds, but the differences are small. The predicted

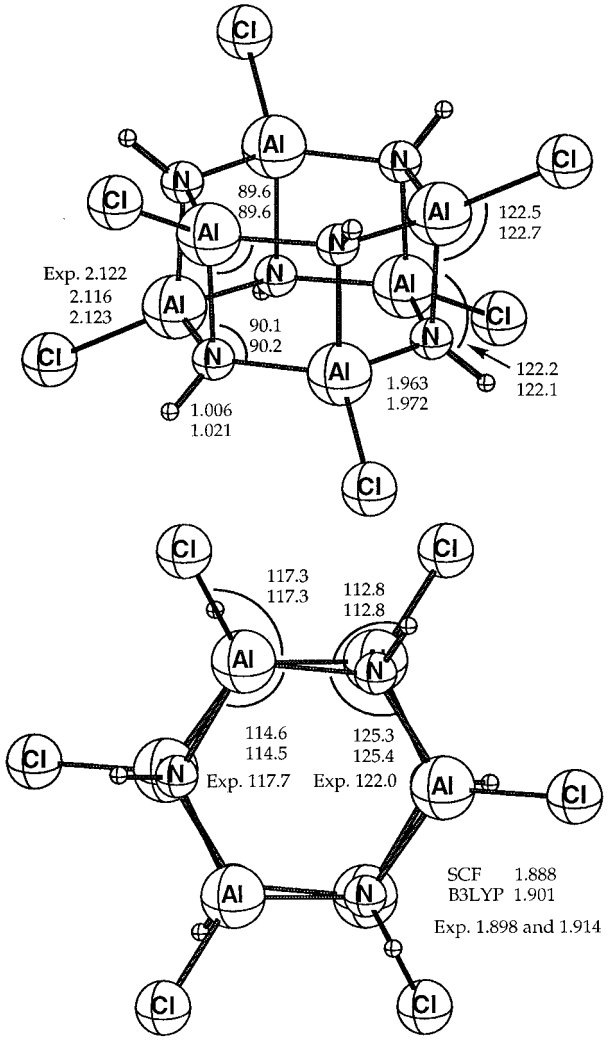

Figure 10. Geometry of $(ClAlNH)_6$.

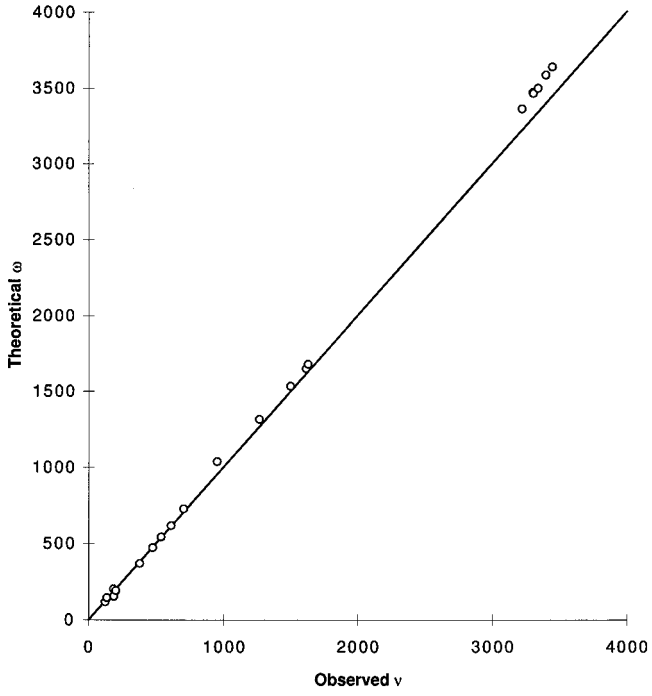

Figure 11. Experimental and theoretical vibrational frequencies.

dissociation enthalpy of the $AlCl_3NH_3$ adduct is 149 kJ mol^{-1}, in agreement with literature values of 133 kJ mol^{-1}. Cl_2AlNH_2 was found to be stable with respect to both dissociation and HCl elimination processes. Both processes are highly endothermic for Cl_2AlNH_2, and formation of ClAlNH and $AlCl_2$ and NH_2 species directly from Cl_2AlNH_2 is improbable. This high thermal stability of Cl_2AlNH_2 is mostly due to the relative instability of the dissociation products, in particular the $AlCl_2$ and NH_2 radicals. The energy difference for the process $Cl_2AlNH_2 \rightleftarrows AlCl_2 + NH_2$ involves not only Al−N bond breaking but also the distortion energy of the fragments, which are evanescent in the gas phase. The Al−N distance in Cl_2AlNH_2 is 0.26 Å shorter, and the Al−N stretch vibrational mode is

Table 7. Theoretical and Experimental Standard Enthalpies (kJ mol^{-1}, 298.15 K, 1 atm) for the Model Reactions

	SCF/DZP	MP2/DZP	B3LYP/DZP	experiment
$H_2 \rightleftarrows 2H$	332.8	403.4	448.5	423.0
$N_2 \rightleftarrows 2N$	417.6	865.2	886.9	941.6
$Cl_2 \rightleftarrows 2Cl$	55.2	189.0	212.6	239.2
$HCl \rightleftarrows H + Cl$	300.8	394.9	420.4	427.8
$2HCl \rightleftarrows H_2 + Cl_2$	213.4	197.4	179.8	184.6
$NH \rightleftarrows N + H$	192.0	281.5	348.1	328.4
$NH \rightleftarrows {}^1/_2N_2 + {}^1/_2H_2$	−183.2	−352.7	−319.6	−358.4
$NH_2 \rightleftarrows N + 2H$	440.4	637.1	737.6	710
$NH_2 \rightleftarrows {}^1/_2N_2 + H_2$	−101.2	−198.9	−154.3	−184.9
$NH_3 \rightleftarrows N + 3H$	756.0	1067.3	1178.3	1157.9
$NH_3 \rightleftarrows {}^1/_2N_2 + {}^3/_2H_2$	48.0	29.6	62.1	45.9
$AlCl \rightleftarrows Al + Cl$	379.2	478.0	482.9	495.4
$AlCl \rightleftarrows Al + {}^1/_2Cl_2$	351.6	383.4	376.6	374.1
$AlCl_3 \rightleftarrows Al + 3Cl$	979.2	1221.1	1196.7	1273.5
$AlCl_3 \rightleftarrows Al + {}^3/_2Cl_2$	896.4	937.5	877.8	909.6
$AlCl_3 \rightleftarrows AlCl + Cl_2$	544.7	554.1	501.2	535.5
$AlCl_3NH_3 \rightleftarrows AlCl_3 + NH_3$	149.1		149.0	133.0

Table 8. B3LYP Level Standard Enthalpies (kJ mol^{-1}), Entropies (J mol^{-1} K^{-1}), and Gibbs Energies (kJ mol^{-1})

	ΔH (298.15)	ΔS (298.15)	ΔG (298.15)
$AlCl_3NH_3 \rightleftarrows HCl + Cl_2AlNH_2$	196.0	132.0	156.7
$AlCl_3NH_3 \rightleftarrows HCl + {}^1/_2(Cl_2AlNH_2)_2$	69.5	36.2	58.7
$AlCl_3NH_3 \rightleftarrows 3HCl + AlN$	1011.8	405.5	890.9
$Cl_2AlNH_2 \rightleftarrows HCl + {}^1/_2(ClAlNH)_2$	125.7	45.4	112.2
$Cl_2AlNH_2 \rightleftarrows HCl + {}^1/_3(ClAlNH)_3$	62.8	16.5	57.9
$Cl_2AlNH_2 \rightleftarrows HCL + {}^1/_4(ClAlNH)_4$	6.4	12.5	10.2
$Cl_2AlNH_2 \rightleftarrows HCl + {}^1/_6(ClAlNH)_6$	−19.8	−27.0	−11.8
$ClAlNH \rightleftarrows HCl + AlN$	389.1	130.1	350.3
$Cl_2AlNH_2 \rightleftarrows 2HCl + AlN$	815.8	273.5	734.2
${}^1/_2\ (Cl_2AlNH_2)_2 \rightleftarrows HCl + {}^1/_4(ClAlNH)_4$	132.9	83.3	108.1
${}^1/_2(Cl_2AlNH_2)_2 \rightleftarrows HCl + {}^1/_2(ClAlNH)_2$	252.2	141.2	210.1
${}^1/_2(Cl_2AlNH_2)_2 \rightleftarrows HCl + {}^1/_6(ClAlNH)_6$	106.7	68.8	86.2
${}^1/_6(ClAlNH)_6 \rightleftarrows HCl + AlN$	836.4	300.5	746.8
${}^1/_4(ClAlNH)_4 \rightleftarrows HCl + AlN$	809.3	286.0	724.1
$AlCl_3NH_3 \rightleftarrows AlCl_3 + NH_3$	149.0	129.1	110.5
$Cl_2AlNH_2 \rightleftarrows AlCl_2 + NH_2$	420.2	162.6	371.7
$ClAlNH \rightleftarrows AlCl + NH$	229.5	129.9	190.8
$Cl_2AlNH_2 \rightleftarrows {}^1/_2(Cl_2AlNH_2)_2$	−126.5	−95.8	−97.9
$ClAlNH \rightleftarrows {}^1/_2(ClAlNH)_2$	−300.9	−98.0	−271.7
$ClAlNH \rightleftarrows {}^1/_3(ClAlNH)_3$	−363.8	−126.9	−326.0
$ClAlNH \rightleftarrows {}^1/_4(ClAlNH)_4$	−420.3	−155.9	−373.8
$ClAlNH \rightleftarrows {}^1/_6(ClAlNH)_6$	−446.5	−170.4	−395.7
$(ClAlNH)_2 \rightleftarrows {}^1/_2(ClAlNH)_4$	−238.6	−115.8	−204.1
$(ClAlNH)_3 \rightleftarrows {}^1/_2(ClAlNH)_6$	−247.9	−130.4	−209.1
$(ClAlNH)_2 \rightleftarrows {}^1/_3(ClAlNH)_6$	−290.3	−144.7	−247.1
$Cl_2AlNH_2 \rightleftarrows AlCl + HCl + {}^1/_2N_2 + {}^1/_2H_2$	336.5	253.2	261.0
$AlCl_3NH_3 \rightleftarrows AlCl + 2HCl + {}^1/_2N + {}^1/_2H_2$	532.5	385.2	417.7
${}^1/_2(Cl_2AlNH_2)_2 \rightleftarrows AlCl + HCl + {}^1/_2N_2 + {}^1/_2H_2$	463.0	349.0	359.0
${}^1/_6(ClAlNH)_6 \rightleftarrows AlCl + {}^1/_2N_2 + {}^1/_2H_2$	356.3	280.2	272.8
${}^1/_4(ClAlNH)_4 \rightleftarrows AlCl + {}^1/_2N_2 + {}^1/_2H_2$	330.1	265.7	250.9
${}^1/_3(ClAlNH)_3 \rightleftarrows AlCl + {}^1/_2N_2 + {}^1/_2H_2$	273.7	236.7	203.1
${}^1/_2(ClAlNH)_2 \rightleftarrows AlCl + {}^1/_2N_2 + {}^1/_2H_2$	210.8	207.8	148.8

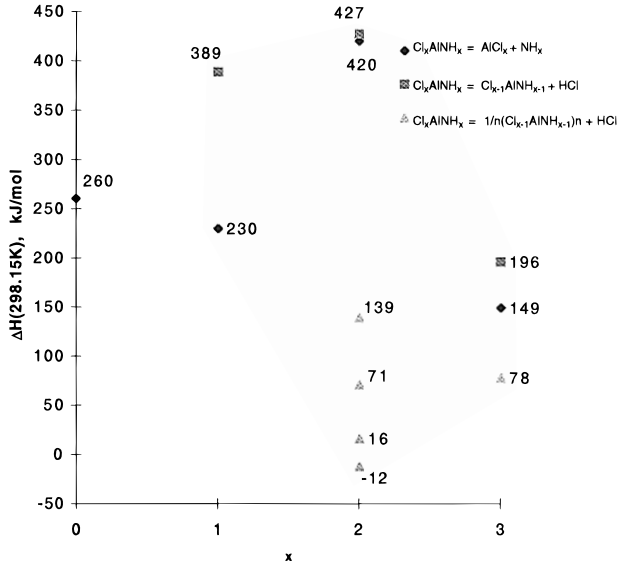

Figure 12. Dissociation processes for Cl_xAlNH_x compounds.

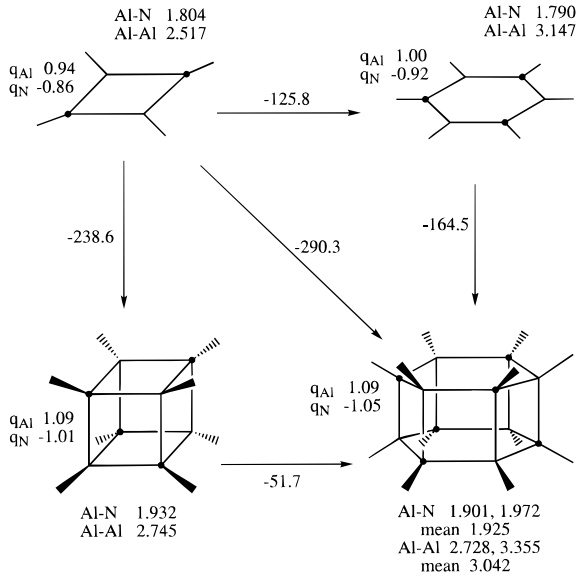

Figure 13. Oligomerization in the gas phase.

400 cm^{-1} larger than those for $AlCl_3NH_3$. These results suggest that the Al−N bond in $AlCl_2NH_2$ is much stronger than in $AlCl_3$-NH_3, in agreement with the theoretical thermodynamic data. From the experimental enthalpy of formation for $AlCl_3NH_3$ and theoretical enthalpies for elimination of HCl, the standard enthalpies of formation for Cl_2AlNH_2 and ClAlNH in the gas phase, ΔH_f (298.15) = −476 and 43 kJ mol^{-1}, respectively, may be estimated.

B. Oligomerization in the Gas Phase. All processes of oligomerization of ClAlNH and Cl_2AlNH_2 compounds are exothermic, but enthropically unfavorable, as shown in Table 8. As the temperature increases, the Gibbs energy of the oligomerization processes grows rapidly. The dimerization energy of Cl_2AlNH_2 is −126.5 kJ mol^{-1} at 298.15 K, making the process $AlCl_3 + NH_3 \rightleftarrows HCl + {}^1/_2(Cl_2AlNH_2)_2$ exothermic. Under standard conditions the $(ClAlNH)_6$ hexagonal and $(ClAlNH)_4$ cube 4-coordinated compounds are more stable than the 3-coordinated dimer $(ClAlNH)_2$ and trimer $(ClAlNH)_3$ (Figure 13). The energies of dimerization of 3-coordinated $(ClAlNH)_2$ and $(ClAlNH)_3$ to form 4-coordinated cube and hexagonal forms, are

$$(ClAlNH)_2 \rightleftarrows {}^1/_2(ClAlNH)_4, \quad \Delta H\,(298.15) = -238.6 \text{ kJ mol}^{-1}$$

$$(ClAlNH)_3 \rightleftarrows {}^1/_2(ClAlNH)_6, \quad \Delta H\,(298.15) = -247.9 \text{ kJ mol}^{-1}$$

The mean value of additional Al−N bond formation is 119 and 83 kJ mol^{-1} per bond, respectively. The lower value for the hexagonal compound compared to the cube is due to the inequivalence in the Al−N bonds: the bond length between two Al_3N_3 rings is 1.956 Å, while in the tetramer the bond length is 1.923 Å. The Al−Al distance in the dimer is short, which leads to high electrostatic repulsion due to high charge separation between Al and N. This leads to an extremely high dimer−trimer enthalpy of reorganization from dimer to trimer for 3-coordinated compounds $(ClAlNH)_2 \rightleftarrows {}^2/_3(ClAlNH)_3$, ΔH (298.15) = −125.8 kJ mol^{-1} where all Al−N, Al−Cl, and N−H bonds are formally preserved and all atoms are coplanar. For the trimer, the Al−N bond is 0.014 Å shorter, but the Al−Cl and N−H bonds are 0.013 and 0.006 Å longer than for the dimer. Similarly, reorganization of the 4-coordinated cube to the hexagonal form, where the Cl and H atoms are distorted from planarity, involves less energy:

$${}^1/_2(ClAlNH)_4 \rightleftarrows {}^1/_3(ClAlNH)_6, \quad \Delta H = -51.7 \text{ kJ mol}^{-1}$$

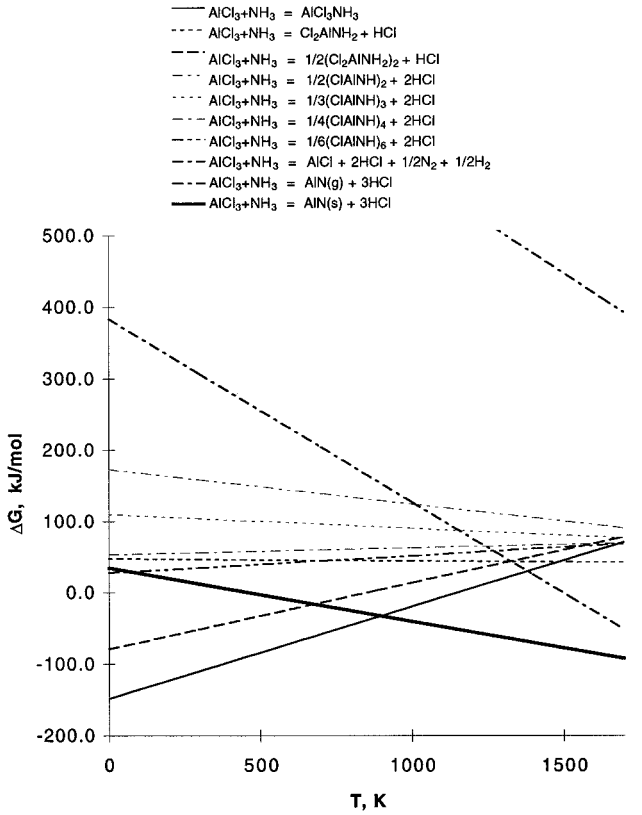

Figure 14. Gibbs energy diagram for the major processes in the CVD of AlN.

C. Thermodynamics of CVD Processes. Before we discuss the thermodynamics of the CVD processes, some comments concerning the experimental details should be made. Usually, the CVD of AlN is carried out using gas flow through a tube with a high temperature gradient. Some laboratories use different source concentrations of $AlCl_3$ and ammonia: from the $AlCl_3NH_3$ adduct to the NH_3-$AlCl_3$ ratio of 3:1. Different carrier gases have been employed in the experimental process:

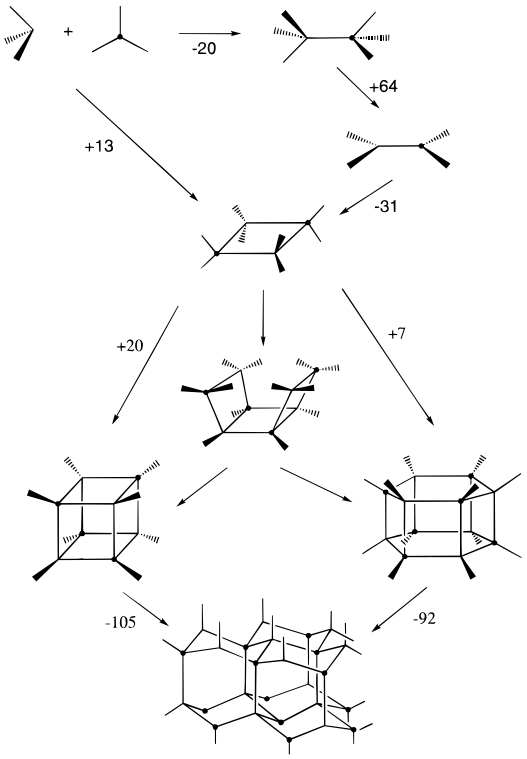

Figure 15. Gibbs energy diagram for the CVD process under 1000 K.

nitrogen, helium, hydrogen, and ammonia. Among these four carrier gases, nitrogen and helium are inert and will not react with the source species. Hydrogen will chemically react with the $AlCl_3$ species to form AlCl and HCl. The role of ammonia is more complicated: it will facilitate formation of the $AlCl_3$-NH_3 adduct, it will form NH_4Cl with HCl, and it may also reduce $AlCl_3$ at the higher temperatures. It should be noted that CVD of AlN is not an equilibrium process under the experimental conditions: there is a gas flow from the mixing zone (460 °C) to the high-temperature zone (700−1100 °C) in the tube. The speed of equilibrium establishment is unknown, and therefore the following thermochemical study is valid only if the assumption that we have equilibrium in each temperature range is correct. For the following thermochemical study we chose a NH_3-$AlCl_3$ ratio of 1:1.

Figure 14 presents the calculated temperature−Gibbs energy dependence for different reactions of vapor $AlCl_3$ and NH_3. Experimental Gibbs energies for the formation of solid aluminum nitride are also given. From this graph we can conclude that the thermodynamically stable forms in the mixture Al-3Cl-N-3H are the $AlCl_3NH_3$(g) adduct (temperatures up to 900 K) and AlN(s) + 3HCl(g) in the temperature range above 900 K. This indicates that the process of AlN deposition will be considerable above 900 K, in agreement with the experimental data. It is known that above 1400 K AlN deposition ceases. This is due to formation of the AlCl(g) + 2HCl(g) + $^1/_2N_2$(g) + $^1/_2H_2$(g) mixture, which is the most stable combination for gaseous species at this temperature. The gas−solid equilibrium is established much slower than the gas phase equilibrium, and therefore, the AlCl(g), HCl(g), N_2(g), and H_2(g) species formed we will leave the reaction zone before equilibrium with solid AlN can be established.

Finally, the Gibbs energy diagram for the CVD process at 1000 K is presented in Figure 15. $(Cl_2AlNH_2)_2$ lies only 13 kJ mol^{-1} higher than the source $AlCl_3$ and NH_3, and $(ClAlNH)_6$ is only 7 kJ mol^{-1} higher than $(Cl_2AlNH_2)_2$, which makes these species the most important substances in the CVD process. The process of HCl elimination from $(Cl_2AlNH_2)_2$ probably goes via the intermediate compound $Cl_6Al_4N_4H_6$, with subsequent conversion to the cube or hexagonal structure. Similar "broken" cube compounds have been observed for organoaluminum derivatives.[35] The energy of formation of solid AlN is very high for both for hexagon and cube compounds. The HCl detachment probably involves formation of intermediates on the surface of AlN.

Acknowledgment. This research was supported by the U.S. National Science Foundation, Grant CHE-9527468. A.Y.T. gratefully acknowledges the REAP (Russian European Asian Program) for the financial support which made possible his stay at the University of Georgia. H.F.B. thanks the Freistaat Bayern and the DAAD for fellowships.

Supporting Information Available: One table with total energies and zero-point vibrational energies for all species investigated, and seven tables with harmonic vibrational frequencies and infrared intensities for Cl_2AlNH_2, ClAlNH, $(Cl_2AlNH_2)_2$, $(ClAlNH)_2$, $(ClAlNH)_3$, $(ClAlNH)_4$, and $(ClAlNH)_6$ (11 pages). See any current masthead page for ordering and Internet access instructions.

JA964163S